Journal of Translational Medicine

RESEARCH Open Access

Engineered sensor actuator modulator as aqueous humor outflow actuator for gene therapy of primary open-angle glaucoma

Samarendra Mohanty[1*], Subrata Batabyal[1], Chinenye Idigo[1], Darryl Narcisse[1], Sanghoon Kim[1], Houssam Al-Saad[1], Michael Carlson[1], Kissaou Tchedre[1] and Adnan Dibas[1]

Abstract

Glaucoma, a blinding eye disease with optic neuropathy, is usually associated with elevated intraocular pressure (IOP). The currently available pharmacological and surgical treatments for glaucoma have significant limitations and side effects, which include systemic reactions to medications, patient non-compliance, eye infections, surgical device failure, and damage to the eye. Here, we present Sensor-Actuator-Modulator (SAM), an engineered double mutant version of the bacterial stretch-activated mechanosensitive channel of large conductance (MscL) that directly senses tension in the membrane lipid bilayer of cells and in response, transiently opens its large nonspecific pore to release cytoplasmic fluid. The heterologously expressed mechanosensitive SAM channel acts as a tension-activated pressure release valve in trabeculocytes. In the trabecular meshwork (TM), SAM is activated by membrane stretch caused by elevated IOP. We have identified several SAM variants that are activated at physiologically relevant pressures. Using this barogenetic technology, we have demonstrated that SAM is functional in cultured TM cells, and successfully transduced in vivo in TM cells by use of AAV2/8. Further, it is effective in enhancing aqueous humor outflow facility leading to lowering the IOP in a mouse model of ocular hypertension.

Keywords Pressure regulator, Intraocular pressure, Glaucoma, Gene therapy, Barogenetics

One sentence summary

Autoregulation of intraocular pressure via expression of a mechanosensitive channel of large conductance in trabecular meshwork serves as a mutation-agnostic gene therapy for glaucoma.

*Correspondence:
Samarendra Mohanty
smohanty@nanoscopetech.com
[1]Nanoscope Technologies, LLC, 1312 Brown Trail, Bedford, TX 76022, USA

Introduction

Cells of different organs in the body undergo a range of mechanical and osmotic pressures which change in various diseases including neurological, cardiovascular, ophthalmological, and renal diseases. Clogging of the outflow pathway in the eyes and brain leads to hypertension and related injury. Glaucoma is usually associated with elevated intraocular pressure (IOP). Vision loss due to glaucoma is the second leading cause of blindness [1]. The currently available pharmacological and surgical treatments for glaucoma have significant limitations and side effects, which include systemic reactions to medications, patient non-compliance, eye infections, surgical device failure, and damage to other structures of the eye [2]. Primary open-angle glaucoma (POAG) is common and is characterized by poor drainage of aqueous humor (AH) through the conventional outflow pathway. Previous studies have shown overexpression of fibrotic proteins [3,4] in glaucomatous trabecular meshwork (TM) is related to increased stiffness of TM along with modulation of TM cell behavior [5,6]. Increased extracellular matrix deposition and cytoskeletal rearrangements of cross-linked actin networks (CLANs) in the glaucomatous TM cause AH outflow resistance [3,7]. Continuous turnover of extracellular matrix (ECM) is required for the maintenance of IOP regulation. This proteinaceous build-up inhibits the translocation of aqueous humor through the TM leading to IOP elevation. Several TM ECM manipulations have been conducted to modulate the outflow facility. The approved drugs address the improvement of drainage through the conventional outflow pathway [2,8] by either reducing AH production (e.g. Beta-blockers [9]) or increasing uveoscleral outflow (e.g. prostaglandins) [8] or TM outflow (Rhopressa [10]).

Though more than a hundred genes have been identified to be associated with glaucoma [11], no single gene is known to account for more than a small fraction of the glaucoma population [12]. Further, since no common convergent pathway(s) have been identified at this point, classical mutation-specific gene replacement/editing approaches [13] would require many therapies to be developed to address various mutations one at a time. The development of a safe effective long-lasting single-dose therapeutic for the ubiquitous treatment of glaucoma would transform the field of ophthalmology. The putative mechanosensitive channel TRPV4 plays a regulatory role in the Ca^{2+}-dependent cytoskeleton rearrangement signaling cascade and its inhibition increases aqueous humor outflow and decreases TM stiffness and IOP [7,14].

The proposed use of a more effective mechanosensitive Sensor-Actuator-Modulator (SAM) channel-based gene therapy is inspired by existing physiological concepts of large pore mechanosensitive channels of Large conductance (MscL) [15–17]. SAM is activated by any mechanical force that causes deformation of the lipid bilayer, such as stretch, pressure/suction, turgor pressure, and ultrasound. Cell contraction and/or relaxation can similarly change the shape of the cells within the TM and Schlemm's canal to promote AH outflow. Although some drugs stimulate outflow in this manner, it may not be sufficient to lower the IOP. Here, we put forth a novel commission for the engineered mechanosensitive channel (SAM) as a virally delivered transgenic pressure modulator in the TM cells of glaucomatous eyes. In the TM, SAM is activated by membrane stretch caused by elevated IOP. Using this barogenetic technology, we have demonstrated that SAM is functional in cultured TM cells, and successfully transduced in vivo in TM cells by use of AAV2/8. Further, we demonstrate effective lowering of the IOP upon SAM transduction in TM in a mouse model of ocular hypertension.

Results

Expression of SAM in transfected trabecular meshwork cells

To evaluate SAM expression, the SAM gene, encoding for 136 amino acids, was codon optimized for mammalian cell expression and C-terminally fused to mCherry (fluorescent reporter). The matrix Gla protein promoter (pMGP) was used to target TM cells [18]. The construct was cloned and confirmed by agarose electrophoresis. The human TM (transformed via SV40) cells were characterized to evaluate the upregulation of TM markers upon Dexamethasone (DEX) treatment. Supplementary Fig. 1 shows enhanced Myocilin, PAI-1, Collagen-IV, and Fibronectin immunostaining in DEX-treated TM cells as compared to the negative control. The Western blot confirmed the upregulation of Fibronectin in DEX-treated TM cells. The TM cells were transduced with AAV8 carried SAM-mCherry and protein expression was determined by confocal microscopy and Western blot. Bright-field image of SAM-mCherry transfected human TM cells is shown in Fig. 1A. The viability of the SAM-transfected TM cells was confirmed by Calcein AM staining (Fig. 1B). The fluorescence (mCherry-reporter) image of human TM cells expressing SAM is shown in Fig. 1C. Further, an anti-SAM antibody was used to evaluate the protein expression and characterization. After transfection of SAM using lipofection or AAV8 (different titers) transduction in cultured human TM cells, the proteins were isolated and subjected to immunoprecipitation using anti-SAM antibody. Figure 1D shows the chemiluminescence Western blot of immunoprecipitated SAM trimers extracted from the human TM cells.

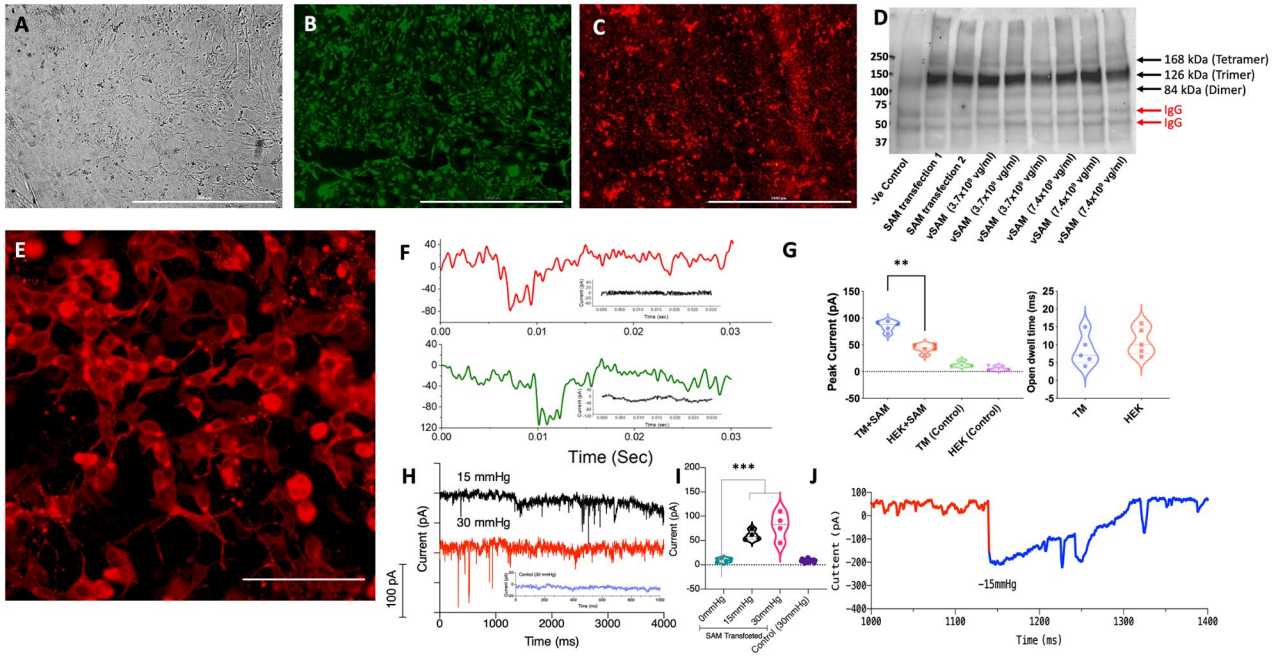

Fig. 1 Expression of SAM-mCherry in transfected trabecular meshwork (TM) cells and kinetics of inward current in SAM-expressing TM cells under hypo-osmotic shock. **(A)** Bright Field image of human TM (Transformed via SV40) cells, **(B)** Calcein image of human TM cells after SAM transfection showing live cells, **(C)** Fluorescence (mCherry-reporter) image of TM cells expressing SAM. Scale bar: 1 mm. **(D)** Western blot confirming SAM (predominantly trimer, estimated MW of trimer = ~ 126 kDa) expression in human TM cells, also shown is non-transfected -ve control. **(E)** Fluorescence (mCherry-reporter) image of HEK cells expressing SAM. Scale bar: 100 µm. **(F)** The inward current profile of a SAM-expressing in HEK 293 (Top: red trace) and rat TM (Bottom, green trace) cell subjected to a hypotonic environment (addition of 20% v/v water). Insets show the respective current trace for non-transfected HEK (top panel: black trace) and TM (bottom panel: black trace) cells (-ve control). **(G)** Comparison of SAM channel peak current and open dwell time in SAM-transfected TM and HEK cells along with the non-transfected cells (-ve control). $N = 5$. Av.± S.D. $^{**}p < 0.01$ (Mann Whitney test). **(H)** The inward current profile of SAM-expressing cells subjected to -15 mmHg (black trace) and −30 mmHg (red trace). The inset (blue trace) shows the current profile of non-transfected cells subjected to -30 mmHg. **(I)** Quantitative comparison of inward current for 2 different hold-pressures as compared to no pressure control in SAM-transfected cell, and -ve control (non-transfected) cell. $N = 4$, Av.± S.D., $^{***}p < 0.001$ (Mann Whitney test). **(J)** SAM-channel activity (blue trace) to sharp (~ 50 ms) pressure changes (up to pressure application: red section of trace)

Functioning of SAM channels in TM cells is different from that in other mammalian cells

To evaluate the functioning of SAM in different mammalian cells, SAM-transfected cells (i.e., HEK and TM, Fig. 1E) and non-transfected (-ve control) cells were subjected to whole cell patch clamp electrophysiology. Channel activity was induced by subjecting the patched cell to a hypo-osmotic shock by adding 20% v/v water (Fig. 1F). The comparison of SAM channel peak current and open dwell time (duration of channel opening) in TM and HEK cells showed that the host membrane greatly affects channel properties (Fig. 1G). Significantly higher SAM-peak current was observed in TM cells as compared to HEK cells. However, no significant changes in open dwell time in TM and HEK cells were observed (Fig. 1G).

Next, automated pressure-clamp electrophysiology was used to measure the effect of varied pressure on SAM-expressing mammalian cells. The cultured cells transfected with SAM were transferred to a patch clamp chamber in which negative pressure was created by use of a suction pump to exert a definite pressure on the cells. Inward current profiles of SAM-expressing cells subjected to -15 mmHg and −30 mmHg are shown in Fig. 1H. Figure 1I shows a quantitative comparison of inward current for 2 different hold-pressures as compared to no pressure control in SAM-transfected cell and non-transfected (-ve control) cell. SAM-channel activity to sharp (~ 50 ms) pressure changes (Fig. 1J) was higher than that during sustained elevated pressure conditions (Fig. 1I).

Intracameral injection of AAV carried SAM-mCherry led to transduction of TM without apoptosis or eliciting immune response

To evaluate SAM expression in-vivo, intracameral injection of AAV2/8-pMGP-SAM-mCherry (vSAM: 6.75×10^{10} vg/eye) was carried out in mice. Intracameral AAV-SAM-mCherry (vSAM) injection in mice led to SAM-mCherry (intrinsic) expression in the iridocorneal junction (Fig. 2A, B). The DEX-only control group (Fig. 2C, D) did not exhibit the characteristic expression. Figure 2E shows a quantitative comparison of

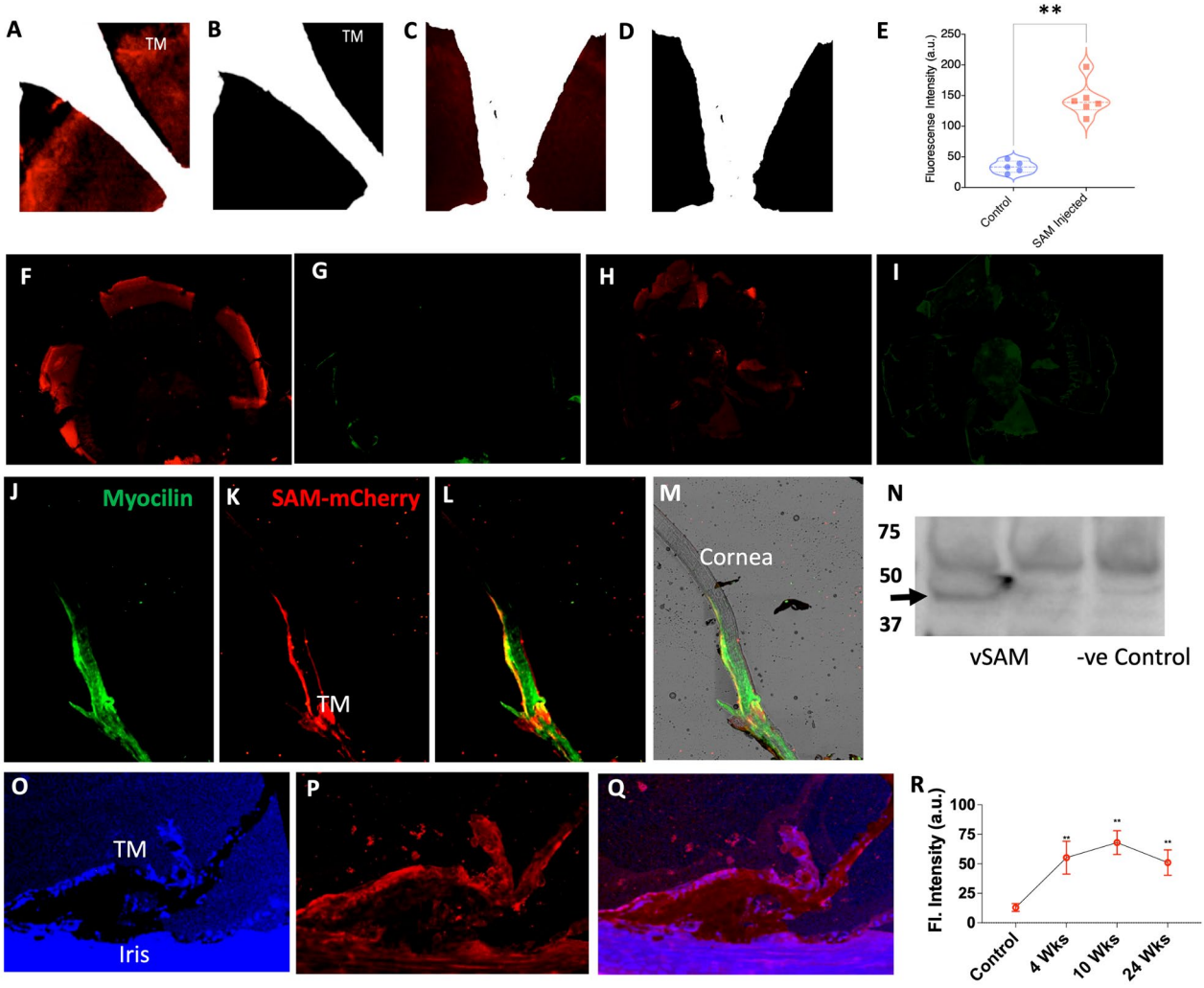

Fig. 2 Intracameral injection of AAV carriedSAM-mCherry led to transduction of trabecular meshwork (TM) in-vivo. Representative fluorescence and Bright field *images of* flat mount anterior segment showing (**A**, **B**) SAM-mCherry (intrinsic) expression in iridocorneal junction in mice 4 weeks post intracameral AAV-SAM-mCherry (vSAM) injection; (**C**, **(D)** DEX-only control group, (**E**) The bar plot showing intensity of mCherry-reporter signal in the TM for SAM-treated and control (PBS) eyes. N = *5*, Av ± SD. $^{**}p < 0.01$ (Mann Whitney test). Fluorescence images of anterior chamber flat mount immunostained with mCherry (red, reporter for SAM) and Caspase-3 (green) for (**F**-**G**) DEX mouse, 10 weeks after vSAM treatment; (**H**-**I**) wild-type -ve control (PBS-injected) mouse. No detectable apoptotic cells in vSAM-treated mice. Confocal Images of iridocorneal regions in the axial sections of the eye transfected by vSAM: **(J)** Myocilin (TM-marker), **(K)** mCherry-reporter, and (L, M) Overlay. **(N)** Western blot confirming SAM (estimated MW = ~ 42 kDa) expression in mice anterior chamber lysate. High-resolution immunostained images of SAM-mCherry expression in TM in mice 24 weeks post intracameral AAV-SAM-mCherry (vSAM) injection: **(O)** DAPI, **(P)** mCherry (red, reporter for SAM), and **(Q)** overlay. **(R)** Pharmacokinetics of SAM using mCherry-reporter fluorescence intensity in the TM, *N* = 6 eyes, Av ± SEM. $^{**}p < 0.01$

fluorescence intensity of mCherry-reporter signal in the TM for SAM-treated and -ve control eyes. To evaluate apoptosis of TM expressing SAM, immunofluorescence imaging of Caspase-3 in an anterior chamber flat mount was carried out. Cells in surrounding tissues, e.g., lens, corneal endothelium were not transduced by SAM as no expression of the reporter (mCherry) protein was observed (Fig. 2F). Figure 2F&G show the SAM-mCherry (red) expression and Caspase-3 staining (green) respectively, 10 weeks after vSAM treatment of DEX-mouse. No detectable apoptotic cell in vSAM-treated mice was observed (Fig. 2G). Figure 2H&I show immunostained images for mCherry (red) and Caspase-3 in wild-type PBS-injected (-ve control) mice. Confocal Images of iridocorneal regions in the axial sections of the eye transfected by vSAM are shown for: TM-marker Myocilin (Fig. 2J), and SAM-mCherry-reporter (Fig. 2K). Overlay of TM-marker and mCherry reporter shows an expression of SAM in TM (Fig. 2L, M). Western blot of anterior chamber lysate from vSAM-injected mice confirms SAM expression (Fig. 2N).

Further, to understand the efficacy of SAM transduction in glaucoma-affected TM cells in vivo, we monitored mCherry reporter fluorescence in TM of IOP-elevated

animal group. High-resolution immunostained images of SAM-mCherry expression in TM in mice 24 weeks post intracameral AAV-SAM-mCherry (vSAM) injection are shown in Fig. 2O-Q. Figure 2R shows the pharmacokinetics of SAM using mCherry-reporter fluorescence intensity in the TM. Stable expression of SAM was observed from 4 weeks of vSAM injection. To evaluate if vSAM injection leads to local immune response, the anterior chamber of SAM-injected mice was immunostained with Iba1 (a marker for microglia) and IFNg (an inflammatory cytokine). Supplementary Fig. 2A-D show no immune response in vSAM-injected eyes as compared to -ve controls. Further, a quantitative comparison of IL-6 in plasma between baseline and after 1 and 10 weeks of vSAM transduction was carried out. As shown in Suppl. Figure 2E, there was no significant change in systemic inflammatory response observed due to vSAM injection.

SAM lowers IOP in a dexamethasone-induced model of Glaucoma, mediated by outflow facility

The progressive IOP elevation in DEX-induced mice [20] was observed as compared to vehicle-applied mice (Fig. 3B). The schematic of the experimental plan for DEX application (for IOP elevation), intracameral injection, IOP measurement, and end-of-study timeline is shown in Fig. 3A. In Fig. 3B, we show elevated IOP in mice (Arms

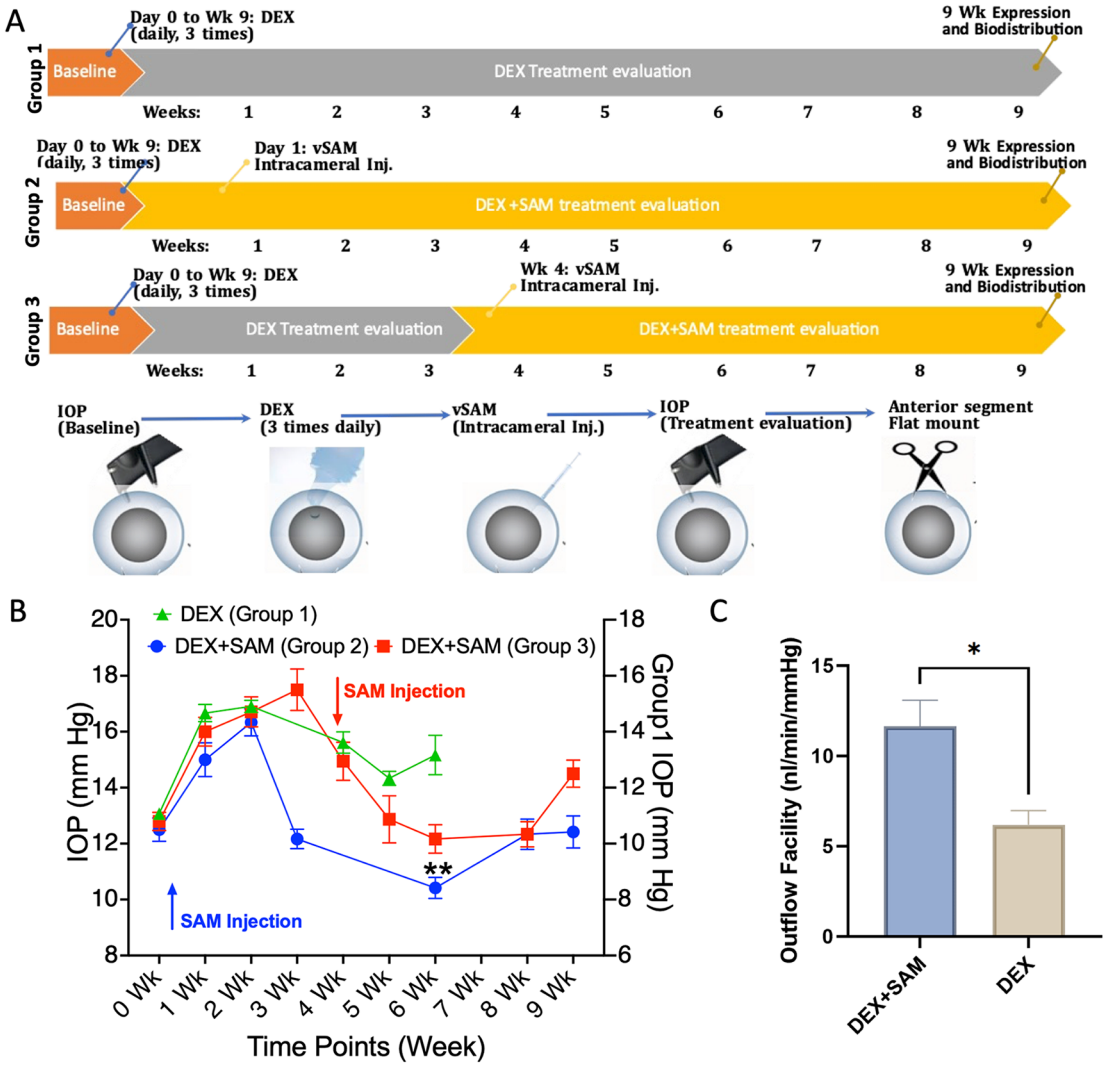

Fig. 3 SAM lowers Intraocular Pressure (IOP) in a Dexamethasone-induced model of Glaucoma. **(A)** Schematic of DEX application, intracameral injection, IOP measurement, and end-of-study timeline. **(B)** Elevated IOP in mice (Groups 1–*3*) treated with topical application of 0.1% DEX, 3 times daily. Group 1 (green): IOP elevat*ion* in mice treated with DEX. Group *2* (blue) and Group 3 (red): IOP in DEX-treated IOP-elevated mice decreases after intracameral injection of vSAM targeted to the TM. *N* = 8 eyes/Arm, Av ± SEM. $^{**}p < 0.01$. Arrows indicate vSAM injection time for Groups 2 and 3. Due to attrition, IOP measurements for DEX-control Group 1 are not available for 7–9 weeks. **(C)** Measured outflow in DEX-treated control vs. SAM-injected DEX-mice, Av ± SD, $^{*}p < 0.05$

1–3) treated with continuous topical application of DEX as early as 1 week. In Group 2, eyes were subjected to intracameral vSAM injection just after baseline IOP measurements. In this Arm, the IOP continued to be elevated due to the DEX application. However, a significant IOP decrease was observed 3 weeks after intracameral injection of vSAM targeted to the TM. In Group 3, intracameral vSAM injection was carried out after observing IOP elevation (at 3 weeks). Immediate reduction in IOP (after vSAM injection) was observed, which can be attributed to the injection itself (though such reduction was not observed in Group 2, which may be due to the dominating effect of IOP elevation by DEX). Similar to Group 2, a statistically significant decrease in IOP as compared to the elevated IOP was observed in the vSAM-injected group in Group 3 (Fig. 3B).

To determine changes in the aqueous outflow facility due to vSAM transduction of TM, aqueous humor hydrodynamics measurement [21] was conducted in anesthetized mice. The linear relationship of pressure versus flow rate in the anesthetized wild-type mouse eye can be seen in Suppl. Figure 3D, leading to the determination of the outflow facility. Figure 3C shows significantly higher measured outflow in SAM-injected DEX-mice as compared to DEX-treated control.

Intracameral injection of SAM protects the RGC as measured by visually evoked potential

To evaluate if intracameral injection of vSAM protects the RGC by lowering IOP, visually evoked potential (VEP) measurements were carried out in DEX-control and DEX+vSAM groups. VEP of DEX-mice and DEX-mice injected with vSAM at a light intensity of 7×10^{13} photons cm^{-2} s^{-1}, 5 weeks after vehicle injection are shown in Fig. 4A & B respectively. As shown in the figure, the VEP amplitude (~15 µV) of DEX-control mice is much lower than the VEP measured in vSAM-treated DEX-mice (~30 µV). The quantitative comparison shows significantly higher VEP amplitude in the vSAM-injected group as compared to DEX-only mice, 5 weeks after injection (Fig. 4C). The mean difference of VEP amplitude between non-transfected and vSAM-injected DEX-mice is shown as Gardner-Altman estimation plot (Fig. 4D).

SAM-induced lowering of IOP enhances RGC survival under glaucomatous condition

Mice eyes were treated with vehicle or vSAM (following 4 weeks of intracameral injection in post-DEX C57BL/6J mice) in Dexamethasone-treated eyes. Figure 4E shows the RBPMS immunostained fluorescence images in the peripheral and central retina of DEX-treated mice eyes injected with vehicle or vSAM. RGCs, labeled with RGC marker RBPMS, were counted to determine the RGC survival. Quantification of RGCs in vSAM and vehicle-injected DEX-mice groups was performed by immunostaining the retinal explant using RGC-specific RBPMS antibody. The number of RGC-positive ($RBPMS^+$ nuclei) cells was quantified in a retinal flat mount. Quantification of RGC counts per mm^2 of the retina shows higher survival in the vSAM-treated group (Fig. 4F).

Optical coherence tomography based monitoring of retinal thickness in vSAM-treated mice

Three-dimensional Optical Coherence Tomographic (OCT) imaging was carried out to monitor any changes in retina structure due to elevated IOP (caused by DEX injection) and the effect of intracameral injection of vSAM. *ImageJ* was used to analyze the SDOCT images. Quantitative comparison of Ganglion cell and Inner plexiform layer (GCIP) thickness measured from B-scan OCT images of retina of wild-type and DEX-induced IOP-elevated mice showed decreased thickness in IOP-elevated mice, which correlated with lower RGC counts (measured by RGC specific RBPMS antibody staining, Fig. 4F). Further, DEX-induced IOP elevated mice without (-SAM) and with vSAM injection shows no statistically significant difference (Supplementary Fig. 4). Furthermore, injection of vSAM in wild-type mice did not cause any detectable change in GCIP thickness, which implies that vSAM injection does not cause any structural damage to the retina in normal or glaucomatous eyes.

Biodistribution of AAV-packaged SAM

The intracamerally injected vSAM mice were euthanized, and the eye and other tissue samples (Mandibular and Mesenteric lymph nodes, testis/ovary, kidney, liver, brain, spleen, lung, and heart) were harvested. The qPCR detection of vector sequences in mice after 5 weeks of intracameral injection of vSAM shows very small or non-detectable quantities of vector in tissues outside of the treated eyes (Supplementary Fig. 5).

Discussion

SAM provides a unique mechanism of action in lowering IOP. SAM, upon mechanical activation, opens a large non-specific pore to release water, ions, and macromolecules [19]. The SAM molecule is autonomous and does not need partners or energy sources to function. SAM intrinsically senses tension in the membrane and gates in direct response to this mechanical tension. Therefore, the expression of SAM in the TM cell membrane provides a unique mechanism of action for the treatment of glaucoma via the lowering of IOP. Figure S6 describes the unique mechanism of action of SAM-transduced TM, wherein in response to elevated IOP, increased transcellular and paracellular transport decreases IOP. Upon increase in IOP, activation of SAM leads to (i) fluid

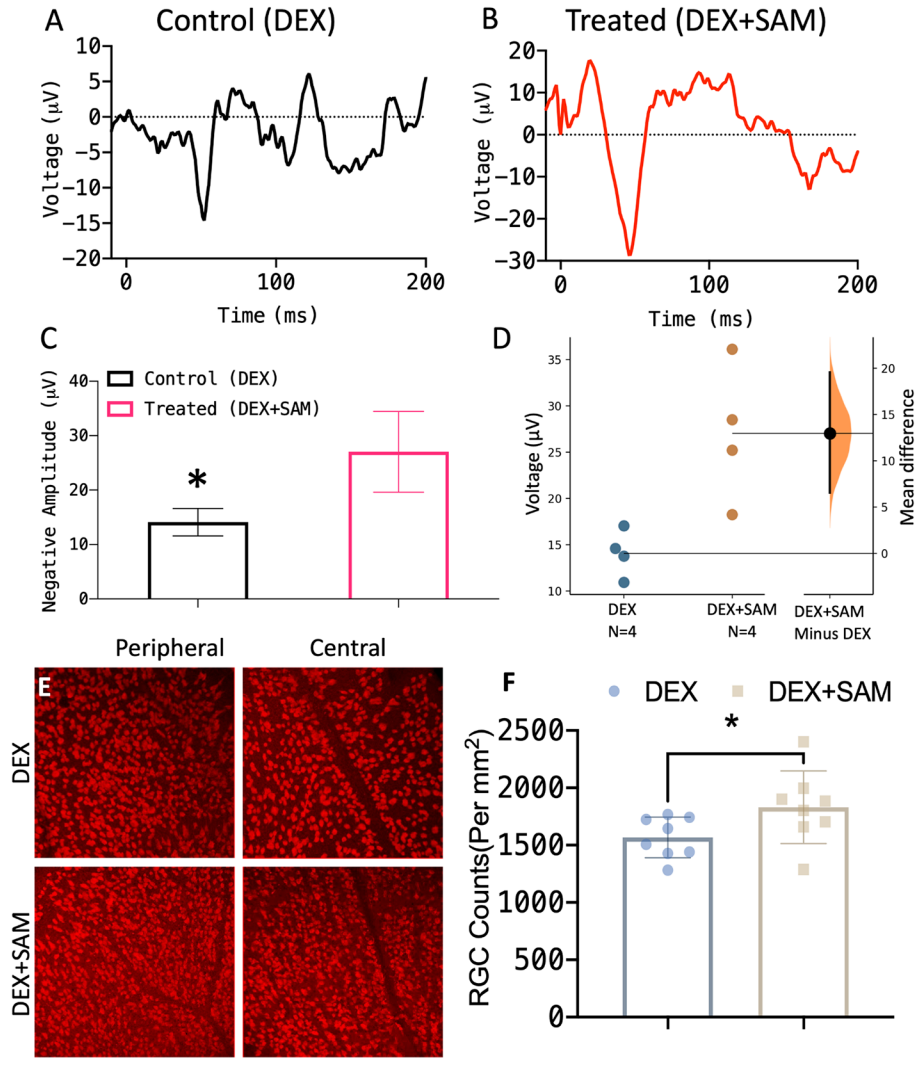

Fig. 4 SAM-induced lowering of IOP was neuroprotective to adult mice RGCs under Glaucomatous condition. Visually evoked potential (VEP) in DEX-mice with and without intracameral injection of AAV-SAM-mCherry (vSAM): **(A)** Representative VEP of DEX-mice, 5 weeks after vehicle injection; **(B)** Representative VEP of DEX-mice injected with vSAM 5 weeks after injection. Light stimulation at 0 ms. **(C)** Quantitative comparison of negative VEP amplitude in DEX-control (black bar) vs. vSAM-injected DEX (pink bar) mice. $N = 4$. Av ± SD. *$p < 0.05$ (Mann Whitney test). **(D)** The mean difference of VEP amplitude between non-transfected and transfected DEX-mice is shown as the Gardner-Altman estimation plot. The curve indicates the resampled distribution of the mean difference, given the observed data. The mean difference was plotted on floating axes on the right as a bootstrap sampling distribution. The mean difference is depicted as a dot; the 95% confidence interval is indicated by the ends of the vertical error bar. **(E)** RBPMS immunostained fluorescence images in peripheral and central retina of DEX-treated mice eyes injected with DEX-only and vSAM-treated (following 4 weeks of intracameral injection in post-DEX C57BL/6J mice). **(F)** Quantification of RGC counts per mm^2 of the retina. RGCs labeled with RGC marker RBPMS, in red, were counted to determine the surviving RGCs. Av ± SD. *$p < 0.05$ (Mann Whitney test)

expulsion through the porous TM cells (transcytosis) into the Schlemm's canal (SC), as observed by an increased outflow facility in SAM-treated mice; and (ii) cell shrinkage widens intercellular spaces (paracytosis) allowing for increase in aqueous humor outflow facility.

Patient-dependent drug treatment protocols of daily doses of eyedrops or oral tablets are problematic due to poor patient compliance. Researchers are developing non-invasive drug-delivery ocular implants; however, patients will still need constant medication and dosage adjustments due to drug unresponsiveness and disease conditions. In POAG, increased IOP is often associated with increased outflow resistance through the TM. However, the existing surgery/drugs address the improvement of drainage through the conventional outflow pathway [22]. The most common glaucoma surgery is a trabeculectomy [23], where an alternative outflow pathway is created by removing a section of the sclera, Schlemm's canal, and TM and fashioning a filtration bleb out of a conjunctival tissue flap. Other surgical methods include laser peripheral iridotomy [24], and drainage device implantation [25]. SAM-based gene therapy exploits the

integration of an exogenous macromolecular pressure sensor and outflow actuator into TM cells that target the site of outflow resistance to regulate IOP.

AAV was chosen as the viral serotype for the delivery of SAM to the TM because literature [26] has shown that AAV2/8 was able to successfully transfect cells of the conventional outflow pathway in mice [27]. In response to elevated IOP, SAM-transduced TM facilitates increased transcellular and paracellular transport as evidenced in AH outflow facility measurements. This is supported by studies showing that when the contractility of TM cells is inhibited (e.g., by nitric oxide donors and Rho kinase inhibitors [28]), the cells change shape, thereby creating more intercellular spaces and consequently improving AH outflow through the TM [2]. At its pressure threshold, SAM can release fluid from TM cells to be cleared through Schlemm's canal. SAM acts as an ideal drainage valve for TM cells because it is a large non-specific pore that does not need any associated proteins or energy sources to assemble and function. Additionally, the resulting decrease in cell volume and size will widen intercellular spaces and facilitate the paracellular flow of aqueous humor.

SAM-based barogenetic gene therapy for POAG focuses on disease phenotype versus a specific genotype. Most gene therapies aim to compensate for a single aberrant gene by introducing a functional copy of the gene into the cell. The existing studies on identifying the gene(s) linked to Glaucoma and therapeutic interventions are genotype-specific such as the MYOC gene (encoding for myocilin) causing some forms of POAG and Rho-Kinase inhibitor-based therapy [6]. However, POAG is heterogeneous and poorly genetically characterized; therefore, the introduction of SAM-gene therapy as an exogenous mechanosensitive modulator provides a unique opportunity to bypass specific gene targets. Cellular recovery after SAM activation may trigger several signaling cascades that could improve TM cell function. In bacteria, the expression of heat shock proteins (HSPs) is upregulated after MscL gating during hypo-osmotic shock [29]. In mouse mutant myocilin-induced glaucoma (a human POAG genotype) the co-expression of protein-folding chaperones (including HSPs) improves outflow facility by preventing mutant myocilin-induced protein aggregation, thereby restoring function to the cells [30]. Therefore, we hypothesize that if SAM activation triggers HSP expression in mutant myocilin-induced glaucoma TM cells, the AH outflow facility would also be improved.

SAM-based gene therapy has many advantages over drugs and surgical treatments. It would provide an opportunity for a long-term treatment not requiring extensive surgical interventions and repeated dosing for IOP management. The safety and efficacy of AAV-mediated gene therapy have been demonstrated in recent clinical trials and eyes, being self-contained, are ideal targets [2]. The use of a tropic AAV delivered-SAM and cell-specific promoters can further minimize the risk of undesired side effects. With viral vector-based delivery, the episomal expression of gene encoding SAM-molecule would allow long-term SAM expression. The dysfunctional turnover of proteins in TM cells of POAG will help maintaining the SAM expression over a long period. If turnover issues are encountered over the long-term, the non-viral gene delivery approach [31] provides a unique opportunity to redose subjects without causing inflammation or immunogenicity. In cases of low SAM expression or in situations that require activation at low ocular pressures, an external ultrasound device [32,33] may be used to stimulate SAM in a non-invasive manner. Though MscL-expressing neurons have been shown to be stimulated by ultrasound [34], it is yet to be shown if heterologously-expressed MscL in TM cells can be modulated by external ultrasound to further enhance the outflow facility.

Several AAV gene therapy preclinical studies have focused on disease phenotype to treat glaucoma [35]. Table S1 lists the Gene target for IOP lowering, Mechanism of action, Genetic manipulation, Gene delivery method, Gene type, and Animal model of Glaucoma. One of the targets involves enzymes that are directly or indirectly involved in enhancing/degrading extracellular matrix by Matrix metalloproteinases (MMPs). Intracameral injection of scAAV2-MMP1 driven by a GRE promoter has been shown to reduce IOP in steroid-induced sheep model [36]. Increased expression of proteins that can induce MMP expression also has been shown to significantly reduce IOP. Examples include plasminogen activator tissue (PLAT) [37], Cycloexogenase-2 [38], prostaglandin F synthase (PGFS) [39], COX-2 and prostaglandin F receptor (*PTGFR*) [40]. Another mechanism of IOP reduction by gene therapy involves disruption of the actin network. Downregulation of RhoA kinase by either siRNA or scAAV2 expressing the dominant-negative RhoA has been shown to cause significant reduction in IOP [36,41]. In contrast, inhibiting RhoA kinase signaling by expression of *Clostridium botulinum* C3 exoenzyme mediating the ADP-ribsoylation of GTP-binding proteins RhoA, B and C leading to the inhibition of the Rho signaling pathway, was efficient in enhancing AH outflow [42]. In addition, upregulation of caldesmon protein that is known to disrupt actin network also enhanced AH outflow [43]. IOP has also been shown to be lowered by modulating AH formation via downregulation of aquaporin-1 [44], carbonic anhydrases [45], β2-adrenergic receptor [46,47], P2Y2 receptor [48], and endothelial nitric oxide synthase [49]. Further, increased expression of stanniocalcin-1, a stress-response protein using scAAV2 has been shown to lower IOP for 6

months in mice [50]. In the current study, we utilized mechanosensitive bacterial channels' transduction in cells of trabecular meshwork to act as a tension activated pressure-release-valve.

Although the mechanosensitive channels derived from different bacteria are highly homologous, they exhibit distinct differences in their structure and function that were capitalized upon to create a SAM variant that would be useful in the treatment of open-angle glaucoma. SAM and its variants are activated at physiologically relevant pressures around normal human IOP of 10–21 mmHg. As SAM activity is triggered solely by the transduction of mechanical force through lipid-protein interactions, amino acid residues that form those interfaces are critical [12]. The barogenetic approach presented in the manuscript can be further optimized by phylogenetic selection of pressure-sensing and modulating channels that exists in nature along with mutation(s) in the molecular system. The screening of channels can be conducted using pressure clamp electrophysiology by application of appropriate pressure modulation as occurs in the eye during elevated intraocular pressure due to glaucoma, pulsatile ocular blood flow or rubbing of eyes. While the data presented here shows IOP lowering over 8 weeks, the efficacy of SAM therapy in modulating IOP over longer term needs to be evaluated. Further, the translational impact of SAM therapy will depend on transduction efficacy of intracamerally delivered vSAM in human. This will require optimization of the delivery vector (rAAV vs. scAVV) and determination of therapeutic dose for optimal efficacy outcome that does not compromise safety. The eye being immune-privileged allow tolerance to viral vector-based gene therapy with a lower risk of immune-rejection compared to other organs. In case of safety events or requirement of redosing due to loss of gene expression because of turnover in TM, non-viral gene delivery [51, 52] may be utilized. Successful translation of SAM barogenetic gene therapy from research to clinical practice will have potential benefits to patients with abnormal pressure dynamics.

Conclusions

The SAM technology described in this manuscript exploits the integration of an exogenous macromolecular pressure sensor and outflow actuator into TM cells to regulate IOP. The development of a safe and effective long-lasting gene therapy for glaucoma has potential to improve the lives of many individuals. While the technology described in this manuscript shows for the first-in-class control of elevated eye pressure in-vivo by use of a bacterial mechanosensitive channel, the SAM system has to be further characterized and optimized for its use in clinical settings. The pressure sensing and modulation approach may find applications within other organs and therapeutic areas involving abnormal changes in osmotic or mechanical pressure.

Materials and methods

Ethics statement

The experimental protocols were approved by the Institutional Animal Care and Use Committee and all experiments were performed in accordance with relevant guidelines and regulations.

Cloning of SAM

The EcMscL gene from the BL21 (DE3) *E.coli* strain, which encodes for a 136 amino acid monomer, was retrieved and codon optimized for mammalian cell expression. SAM gene sequence is a double mutant (I113L, I70E) of EcMscL. The gene sequence was codon optimized for mammalian expression before synthesis. The gene was put under the control of a TM-specific promoter. Several studies have shown that in the eye matrix Gla protein (MGP) is preferentially expressed in TM cells and its promoter sequence has been used to target gene expression. The MGP promoter sequence (pMGP) located on chromosome 12 was identified by using the primers [18] to run an alignment search against the reverse complement strand of the human genome GRCh38.p12. The resulting 576 bp promoter sequence was placed on the 5' end of the SAM gene. A fused fluorescent reporter was chosen to act as a visual marker of gene expression and membrane localization. As SAM is a homo-oligomer and needs to assemble into a functional complex postranslationally, a strictly monomeric fluorescent protein had to be chosen to avoid any disruptive interactions. To this end, the monomeric fluorescent protein, mCherry, was C-terminally fused to SAM. The gene was inserted into a pAAV-MCS vector backbone by restriction digestion and ligation (T4 DNA Ligase).

Production of AAV carried SAM

AAV carried SAM production was carried out using the triple plasmid transfection method. HEK293 cells were cultured and transfected with a mixture of DNA (Rep-Cap, transfer, and helper plasmids), polyethylenimine, polyethylene glycol (PEG), and Dulbecco's Modified Eagle Medium (DMEM). After incubation at 37 °C for 72 h, cells were trypsinized and lysed. The virus was purified using FPLC chromatography [53]. Viral vectors were resuspended in PBS and titrated to a concentration of 1×10^{13} vg/ml. Vector genome copies were measured by qPCR amplification and SDS-PAGE gel electrophoresis was used to determine sample purity.

HEK293 cell culture

HEK293 cells were grown in flasks in 1.5 mL of Dulbecco's modified Eagle's medium (DMEM) with 4.5 g/L

glucose, L-glutamine and sodium pyruvate, 10% fetal bovine serum, 100 U/mL penicillin, and 100 µg/mL streptomycin sulfate and incubated in a humidified 5% CO^2 environment at 37 °C. A day before transfection, cells were plated in 35 mm Petri dishes in 1.5 ml of media and incubated at 37 °C until ~ 80% confluency.

Corneoscleral culture from rat

Following established dissection procedure [54], the anterior segment from the embryonic eyes of the rat was cut into small explants. After cellular dissociation1.33% collagenase (30–45 min), followed by Trypsin-EDTA (20 min), the corneoscleral cells were seeded onto a poly-D-lysine pre-coated Petri dish. 10% fetal bovine serum was used for the TM cell culture and was changed every 2–3 days. The TM cells were cultured at 37 °C in 5% CO_2 in a humidified atmosphere.

Human TM cell culture

Primary human TM cells (Cell Applications Inc), maintained in DMEM supplemented with 10% FBS and antibiotics, were cultured in Petri dishes. Passages 1 through 4 were used for quantification of transduction efficiency. Analysis of myocilin expression in these cells following dexamethasone treatment showed a reliable increase as reported in the literature [54].

In-vitro transfection

jetPRIME (Polyplus Transfection) was used to deliver 2 µg of SAM-mCherry plasmid DNA to each dish. The plasmid DNA was added to 200 µl of jetPRIME buffer and then vortexed for 10 s. Then, 8 µl of jetPRIME was added and the solution was left to sit at room temperature for 10 min. The solution was then added to the cells and the sample was incubated at 37 °C for 2 h. After 2 h, the growth medium was exchanged for fresh media and incubated at 37 °C for another 48 h. At this time, fluorescence microscopy of live cells was used to confirm the successful transfection and expression of the fluorescent reporter (mCherry).

Fluorescence Confocal Microscopy

Confocal Fluorescence imaging (Olympus FluoView 1000) on an upright microscope platform was carried out to confirm the successful transfection and expression of the fluorescent reporter (mCherry) linked to the SAM gene in cells.

Patch clamp Electrophysiology

The functioning and response of SAM-expressing cells to osmotic pressure were measured by recording electrophysiological measurements from whole cell patches of HEK293 and TM cells. The patch-clamp recording setup includes an inverted Nikon fluorescence microscope (TS 100) platform using an amplifier system (Axon Multiclamp 700B, Molecular Devices). Micropipettes were pulled using a two-stage pipette puller (Narshinghe) to attain resistance of 3 to 5 MΩ when filled with a solution containing (in mM) 130 K-Gluoconate, 7 KCl, 2 NaCl, 1 $MgCl_2$, 0.4 EGTA, 10 HEPES, 2 ATP-Mg, 0.3 GTP-Tris and 20 sucrose. The micropipette-electrode was mounted on a micromanipulator. The extracellular solution contained (in mM): 150 NaCl, 10 Glucose, 5 KCl, 2 $CaCl_2$, and 1 $MgCl_2$ was buffered with 10 mM HEPES (pH 7.3). The transfected cells were identified by observing the mCherry expression under green excitation light. Inward currents were measured while holding cells in a voltage clamp at -70 mV. The electrophysiological signals from the amplifier were digitized using Digidata 1440 (Molecular devices), interfaced with patch-clamp software (Clampex, Molecular Devices). pClamp 10 software was used for data analysis. SAM channel activity was induced by subjecting the patched cell to a hypo-osmotic shock by adding of 20% v/v water. A stable gigaohm seal was achieved and the current traces show channel activity only after the hypo-osmotic shock.

Automated pressure-clamp Electrophysiology

The functioning and response of SAM-expressing cells to pressure clamp were assessed by recording electrophysiological signals from whole-cell patches using the Port-a-Patch system (Nanion, Germany). Planar patch-clamp chips with a chip resistance of 2–3.5 MΩ were used. The internal solution consisted of 10 mM KCl, 10 mM NaCl, 110 mM K-Fluoride, 10 mM EGTA, 10 mM HEPES/KOH, and pH 7.2. The external solution consisted of 4 mM KCl, 140 mM NaCl, 1 mM $MgCl_2$, 2 mM $CaCl_2$, 5 mM D-Glucose monohydrate, 10 mM HEPES/NaOH, Ph 7.4. The seal resistance was typically 1GΩ. The pressure was introduced by SuctionControl Pro (Nanion). The electrophysiological signals from the amplifier (Axon Multiclamp 700B, Molecular Devices) were digitized using Digidata 1440 (Molecular Devices).

Measurement of visually evoked potential (VEP)

The mice were dark-adapted overnight and anesthetized with an intraperitoneal injection of a mixture of Ketamine (90 mg/kg), Xylazine (10 mg/kg), and Acepromazine (0.5 mg/kg). The VEP measurement was carried out in the dark using dim red light. Using the surgical tools, the skull was exposed, and craniotomy was performed by drilling a hole for the recording electrode to access the V1 (AP = −3.0 mm, and ML = +2.5 mm relative to bregma) area of the Visual cortex. The mouse was placed on the stereotaxic unit and the ground electrode was subcutaneously placed in the tail. The reference electrode was placed at AP = +2.5 mm and ML = −1.5 mm. Light flash-VEPs were elicited by a white LED Stimulator

providing stimulus with a stimulus rate of 1 Hz and stimulus duration of 1 ms. Signals were amplified through a Built-In Bias Drive Amplifier, Analog-to-digital converters (ADCs) with a built-in programmable gain amplifier (PGA). A high-pass filter at 5 Hz and a low-pass filter at 250 Hz with a 60 Hz notch filter. Acquisitions were performed at a 1 kHz sampling rate. VEPs from a sequence of 15 strobe light flashes were averaged to obtain the final waveform.

Spectral-domain (SD) optical coherence tomography imaging

Optical Coherence Tomographic (OCT) imaging is a standard ophthalmic assessment tool that provides quantitative measurements of the anterior segment and retina instead of subjective evaluation. Optical sectioning/imaging using SDOCT was carried out to monitor any changes in ocular structure due to intracameral injection of vSAM or vehicle control. Animals were anesthetized using a mixture of Ketamine/Xylazine/Acepromazine. For dilating the pupil, a drop of Tropicamide was topically applied to the eye. SDOCT images of the retina after intracameral injection of vSAM in mice were compared to the images before injection. The retinal thickness measurements were made from the OCT B-scan images using ImageJ.

Experimental animal groups

Dexamethasone-treated adult (>8 weeks old) C57BL/6J mice (strain 000664, The Jackson Laboratory) were used as a glaucoma model [20]. Wild-type mice were used for monitoring the effect of SAM injection in DEX-induced IOP-elevated mice. Elevated IOP in mice was achieved by topical application of 0.1% dexamethasone (DEX), 3 times daily. For monitoring the treatment effect of vSAM, 2 different wild-type mice groups were used. Group 1 consisted of DEX-treated control mice (without SAM injection). Group 2 consisted of mice with vSAM injection at day 1 in DEX mice, and Group 3 comprised of vSAM injection at 4 weeks after initiation of DEX application. DEX treatment protocol (0.1% dexamethasone topical, 3 times daily, 7 days a week) was followed for all three Arms during the whole course of the study.

Intracameral injections

Anesthetized mice (intraperitoneal injection with a mixture of 90 mg/kg ketamine, 10 mg/kg xylazine, and 0.5 mg/kg acepromazine) were injected with virus intracamerally. Under a surgical microscope, a 34 gauge needle was inserted into the cornea, anterior of the iridocorneal angle, and vSAM was delivered at an infusion rate of 1 µl/min. After the procedure, antibiotics were applied to the mouse eye.

IOP monitoring

For IOP measurement, the mouse was placed on a wire cage and allowed ~ 1 min of resting time. The tonometer (Tonovet Plus, iCARE) was loaded with a new probe allowing it for self-calibration. The Tonovet was positioned parallel to the eye with a distance of about half an inch and aimed at the center of the cornea. The IOP was measured in the afternoons. Three trials of IOP measurement were carried out, each trial consisting of 6 readings.

Measurement of aqueous outflow facility

The apparatus for assessments of aqueous humor hydrodynamics is shown in Suppl. Figure 3 A. To measure the aqueous outflow facility, the mice were anesthetized. The anterior chamber of the mouse eye is cannulated by using a 32-gauge steel needle (Suppl. Figure 3B), which was connected to a flow-through pressure transducer for the continuous determination of pressure within the system. The pressure–time trace was obtained from a single experiment. In the anesthetized animal, the pressure was monitored continuously as the Flow rate was set at different rates (Suppl. Figure 3 C). The pump was stopped, and the circuit opened to the manometer, which was then rapidly lowered to re-establish baseline pressure. After this, the circuit was closed again, the animal was euthanatized, perfusion was resumed, and the pressure was monitored to determine the outflow facility.

Harvesting tissue

Mice were euthanized 35 d post-injection in a CO_2 gas chamber and spinal dislocation. The eyes were fixed in 4%PFA at 4 °C overnight, rinsed with PBS, and kept frozen. For biodistribution studies, other vital tissues were kept frozen in the 1.8 ml cryovials and stored at -80 °C. Each vial was properly labeled with an animal identification number, date of extraction, and name of the organ.

Tissue sectioning

Enucleated mouse eyeballs were fixed in 4% PFA at 4 °C overnight followed by storage in 1X PBS. The eyeballs were treated with 30% sucrose and embedded in an optimal cutting temperature (OCT) embedding compound (Tissue-Tek OCT; Electron Microscopy Sciences, Hatfield, PA). For immunostaining, the eyeballs were cryosectioned at 20 µm thickness (Microtome, Microm).

Western blot analysis

Antibodies against fibronectin and mCherry were used to test for protein localization. After fluorescence imaging, cells were lysed, the membrane and cytoplasmic fractions separated by centrifugation, and run on an SDS-PAGE gel. Protein bands were transferred to a nitrocellulose/PVD membrane for immunostaining.

Immunostaining and imaging

For immunostaining, the cells, flat mount, and tissue slices were fixed in 4% PFA at 4°C, which was replaced with 1X PBS. The nonspecific binding of antibodies was blocked by 4% serum for 60 minutes and washed with washing solution three times. The samples were then incubated at 4°C overnight with anti-mCherry (1: 500 dilution), anti-Myocilin, anti-Collagen-IV, anti-PAI-1, anti-Fibronectin (TM-markers), or RBPMS (RGC marker). After washing the samples with 0.5% TritonX-100 solution three times, secondary antibodies were added to the samples for incubation (one hour at room temperature). The samples were stained with nuclear stain DAPI (4', 6-diamidino-2-phenylindole) dye at room temperature for 30 min, rinsed in PBS, and then mounted onto slides in a mounting medium.

Images were taken by confocal microscope (Olympus Fluoview FV1000, Olympus, Center Valley, PA). Image analysis was performed using ImageJ software. Expression of SAM-reporter (mCherry) in TM was carried out in animals injected with vSAM and was compared to control.

DNA extraction and qPCR

Genomic DNA was extracted from tissue samples using the Phenol/chloroform DNA extraction technique [17] and using the Thermofisher Scientific GeneJET Genomic DNA Purification Kit (cat# K0722) according to the manufacturer's protocol. qPCR was performed using Takara AAVpro™ Titration kit standard (cat# 6233) and Fisher Scientific Company's Master Mix, qPCR (Applied Biosystems), and Power Up SYBR Green Master Mix (cat# A25776). 50X Primer Mix was prepared as follows: AAV Forward ITR Primer 5 µl, AAV Reverse ITR primer 5 µl, water 15 µl. The qPCR reaction mix consisted of: SYBR green Premix 12.5 µl, 50X Primer Mix 0.5 µl, water 7 µl, and template DNA (~10 ng) 5 µl. Real-time PCR was performed on the Applied Biosystems QuantStudio 3 real-time PCR System (Applied Biosystems) using assays specific for ITR. Samples were analyzed in duplicate for vector copy number/ng DNA by the Absolute Quantification method using standard curves. Preparation of the standard curve was performed following the manufacturer reference guide.

Statistics

Image processing and analysis were performed using NIH ImageJ software. GraphPad Prism was used to analyze the data. The data were plotted as mean ± SD or SEM. Statistically significant difference analyses were carried out by t-test. In case of low sample size ($N<6$), non-parametric Mann Whitney test was performed. $P<0.05$ was considered statistically significant.

Supplementary Information

The online version contains supplementary material available at https://doi.org/10.1186/s12967-024-05581-1.

Supplementary Material 1

Acknowledgements

The authors would like to thank Dr. Cameron Millar, UNT Health Science Center for help with the outflow measurement setup.

Author contributions

SM designed and supervised the experiments. SB performed patch clamp experiments, imaging, and data analysis. CI designed the construct, DN participated in plasmid purification/production of the vector, SK performed the OCT imaging, HA performed IOP measurement, MC performed electrophysiology (VEP) assessments, and KT performed sectioning, and biodistribution. AD performed cell culture and Western blot. All authors participated in discussion, and data analysis and contributed to the preparation of the manuscript.

Funding

National Eye Institute R44EY033626.

Data availability

All data are available in the main text or the supplementary materials.

Declarations

Competing interests

SM has an equity interest in Nanoscope Technologies, LLC.

Received: 22 May 2024 / Accepted: 6 August 2024
Published online: 28 August 2024

References

1. Tham Y-C, Li X, Wong TY, Quigley HA, Aung T, Cheng C-Y. Global prevalence of glaucoma and projections of glaucoma burden through 2040: a systematic review and meta-analysis. Ophthalmology. 2014;121:2081–90.
2. Kaufman PL, Mohr ME, Riccomini SP, Rasmussen CA. Glaucoma drugs in the pipeline. Asia-Pacific J Ophthalmol. 2018;7:345–51.
3. Wang C, Li L, Liu Z. Experimental research on the relationship between the stiffness and the expressions of fibronectin proteins and adaptor proteins of rat trabecular meshwork cells. BMC Ophthalmol. 2017;17:268.
4. Raghunathan VK, et al. Glaucomatous cell derived matrices differentially modulate non-glaucomatous trabecular meshwork cellular behavior. Acta Biomater. 2018;71:444–59.
5. Yoo H et al. Simvastatin attenuates glucocorticoid-induced human trabecular meshwork cell dysfunction via YAP/TAZ inactivation. Curr Eye Res, 1–14 (2023).
6. Acott TS, Vranka JA, Keller KE, Raghunathan V, Kelley MJ. Normal and glaucomatous outflow regulation. Prog Retin Eye Res. 2021;82:100897.
7. Bermudez JY, Montecchi-Palmer M, Mao W, Clark AF. Cross-linked actin networks (CLANs) in glaucoma. Exp Eye Res. 2017;159:16–22.
8. Challa P, Arnold JJ. Rho-kinase inhibitors offer a new approach in the treatment of glaucoma. Expert Opin Investig Drugs. 2014;23:81–95.
9. Hayreh SS, Podhajsky P, Zimmerman MB. Beta-blocker eyedrops and nocturnal arterial hypotension. Am J Ophthalmol. 1999;128:301–9.
10. Hoy SM. Netarsudil ophthalmic solution 0.02%: first global approval. Drugs. 2018;78:389–96.
11. Youngblood H, Hauser MA, Liu Y. Update on the genetics of primary open-angle glaucoma. Exp Eye Res. 2019;188:107795.
12. Zukerman R, Harris A, Verticchio Vercellin A, Siesky B, Pasquale LR, Ciulla TA. Molecular genetics of glaucoma: subtype and ethnicity considerations. Genes. 2020;12:55.
13. Jain A, et al. CRISPR-Cas9–based treatment of myocilin-associated glaucoma. Proc Natl Acad Sci. 2017;114:11199–204.

14. Ryskamp DA, et al. TRPV4 regulates calcium homeostasis, cytoskeletal remodeling, conventional outflow and intraocular pressure in the mammalian eye. Sci Rep. 2016;6:1–15.
15. Sukharev SI, Blount P, Martinac B, Blattner FR, Kung C. A large-conductance mechanosensitive channel in E. Coli encoded by mscL alone. Nature. 1994;368:265–8.
16. Blount P, Iscla I. Life with bacterial mechanosensitive channels, from discovery to physiology to pharmacological target. Microbiol Mol Biol Rev. 2020;84:e00055–00019.
17. Heureaux J, Chen D, Murray VL, Deng CX, Liu AP. Activation of a bacterial mechanosensitive channel in mammalian cells by cytoskeletal stress. Cell Mol Bioeng. 2014;7:307–19.
18. Liton PB, Liu X, Stamer WD, Challa P, Epstein DL, Gonzalez P. Specific targeting of gene expression to a subset of human trabecular meshwork cells using the chitinase 3-like 1 promoter. Investig Ophthalmol Vis Sci. 2005;46:183–90.
19. Perozo E, Cortes DM, Sompornpisut P, Kloda A, Martinac B. Open channel structure of MscL and the gating mechanism of mechanosensitive channels. Nature. 2002;418:942–8.
20. Zode GS, et al. Ocular-specific ER stress reduction rescues glaucoma in murine glucocorticoid-induced glaucoma. J Clin Investig. 2014;124:1956–65.
21. Shepard AR, Millar JC, Pang I-H, Jacobson N, Wang W-H, Clark AF. Adenoviral gene transfer of active human transforming growth factor-β2 elevates intraocular pressure and reduces outflow facility in rodent eyes. Investig Ophthalmol Vis Sci. 2010;51:2067–76.
22. Sharif NA. Therapeutic drugs and devices for tackling ocular hypertension and glaucoma, and need for neuroprotection and cytoprotective therapies. Front Pharmacol. 2021;12:729249.
23. Watson PG, Grierson I. The place of trabeculectomy in the treatment of glaucoma. Ophthalmology. 1981;88:175–96.
24. Ang LP, Aung T, Chew PT. Acute primary angle closure in an Asian population: long-term outcome of the fellow eye after prophylactic laser peripheral iridotomy. Ophthalmology. 2000;107:2092–6.
25. Greenfield DS, Tello C, Budenz DL, Liebmann JM, Ritch R. Aqueous misdirection after glaucoma drainage device implantation. Ophthalmology. 1999;106:1035–40.
26. Mao W, Liu Y, Mody A, Montecchi-Palmer M, Wordinger RJ, Clark. A. F. characterization of a spontaneously immortalized bovine trabecular meshwork cell line. Exp Eye Res. 2012;105:53–9.
27. Johnson TV, Tomarev SI. Rodent models of glaucoma. Brain Res Bull. 2010;81:349–58.
28. Wang SK, Chang RT. An emerging treatment option for glaucoma: rho kinase inhibitors. Clin Ophthalmol (Auckland NZ). 2014;8:883.
29. Jones SE, Naik RR, Stone MO. Use of small fluorescent molecules to monitor channel activity. Biochem Biophys Res Commun. 2000;279:208–12.
30. Kasetti RB, Phan TN, Millar JC, Zode GS. Expression of mutant myocilin induces abnormal intracellular accumulation of selected extracellular matrix proteins in the trabecular meshwork. Investig Ophthalmol Vis Sci. 2016;57:6058–69.
31. Hangai M, Tanihara H, Honda Y, Kaneda Y. Introduction of DNA into the rat and primate trabecular meshwork by fusogenic liposomes. Investig Ophthalmol Vis Sci. 1998;39:509–16.
32. Coleman DJ, et al. Therapeutic ultrasound in the treatment of glaucoma: II. Clinical applications. Ophthalmology. 1985;92:347–53.
33. Silverman RH, Vogelsang B, Rondeau MJ, Coleman DJ. Therapeutic ultrasound for the treatment of glaucoma. Am J Ophthalmol. 1991;111:327–37.
34. Ye J, et al. Ultrasonic control of neural activity through activation of the mechanosensitive channel MscL. Nano Lett. 2018;18:4148–55.
35. Castro B, Steel JC, Layton CJ. AAV-mediated gene therapies for glaucoma and uveitis: are we there yet? Expert Rev Mol Med. 2024;26:e9.
36. Borrás T, Buie L, Spiga MG. Inducible scAAV2. GRE. MMP1 lowers IOP long-term in a large animal model for steroid-induced glaucoma gene therapy. Gene Ther. 2016;23:438–49.
37. Kumar S, Shah S, Tang HM, Smith M, Borrás T, Danias J. Tissue plasminogen activator in trabecular meshwork attenuates steroid induced outflow resistance in mice. PLoS ONE. 2013;8:e72447.
38. Barraza RA, McLaren JW, Poeschla EM. Prostaglandin pathway gene therapy for sustained reduction of intraocular pressure. Mol Ther. 2010;18:491–501.
39. Lee ES, et al. Prospects for lentiviral vector mediated prostaglandin F synthase gene delivery in monkey eyes in vivo. Curr Eye Res. 2014;39:859–70.
40. Chern KJ, Nettesheim ER, Reid CA, Li NW, Marcoe GJ, Lipinski DM. Prostaglandin-based rAAV-mediated glaucoma gene therapy in Brown Norway rats. Commun Biology. 2022;5:1169.
41. Liu Q, Wu K, Qiu X, Yang Y, Lin X, Yu M. siRNA silencing of gene expression in trabecular meshwork: RhoA siRNA reduces IOP in mice. Curr Mol Med. 2012;12:1015–27.
42. Liu X, et al. The effect of C3 transgene expression on actin and cellular adhesions in cultured human trabecular meshwork cells and on outflow facility in organ cultured monkey eyes. Mol Vis. 2005;11:1112–21.
43. Gabelt BAT, Kaufman PL. Bimatoprost for glaucoma therapy: pharmacology, clinical efficacy and controversy. Expert Rev Ophthalmol. 2006;1:141–58.
44. Wu J, et al. Gene therapy for glaucoma by ciliary body aquaporin 1 disruption using CRISPR-Cas9. Mol Ther. 2020;28:820–9.
45. Jimenez A, Sesto A, Pintor J, Mediero A, Peral A, de Buitrago GG. RNAi: a new strategy for treating ocular hypertension silencing carbonic anhydrases. Investig Ophthalmol Vis Sci. 2006;47:405–405.
46. Loma P, Guzman-Aranguez A, de Lara MJP, Pintor J. Beta2 adrenergic receptor silencing change intraocular pressure in New Zealand rabbits. J Optometry. 2018;11:69–74.
47. Moreno-Montañés J, et al. Phase I clinical trial of SYL040012, a small interfering RNA targeting β-adrenergic receptor 2, for lowering intraocular pressure. Mol Ther. 2014;22:226–32.
48. Martin-Gil A, de Lara MJP, Crooke A, Santano C, Peral A, Pintor J. Silencing of P2Y2 receptors reduces intraocular pressure in New Zealand rabbits. Br J Pharmacol. 2012;165:1163–72.
49. You Y, et al. Progesterone promotes endothelial nitric oxide synthase expression through enhancing nuclear progesterone receptor-SP-1 formation. Am J Physiol Heart Circ Physiol. 2020;319:H341–8.
50. Roddy GW, et al. Transgene expression of Stanniocalcin-1 provides sustained intraocular pressure reduction by increasing outflow facility. PLoS ONE. 2022;17:e0269261.
51. Batabyal S, Gajjeraman S, Tchedre K, Dibas A, Wright W, Mohanty S. Near-Infrared laser-based spatially targeted nano-enhanced optical delivery of therapeutic genes to degenerated retina. Mol Therapy Methods Clin Dev. 2020;17:758–70.
52. Batabyal S, Kim S, Wright W, Mohanty S. Layer-specific nanophotonic delivery of therapeutic opsin-encoding genes into retina. Exp Eye Res. 2021;205:108444.
53. Burova E, Ioffe E. Chromatographic purification of recombinant adenoviral and adeno-associated viral vectors: methods and implications. Gene Ther. 2005;12(Suppl 1):S5–17.
54. Keller KE, et al. Consensus recommendations for trabecular meshwork cell isolation, characterization and culture. Exp Eye Res. 2018;171:164–73.

Publisher's Note